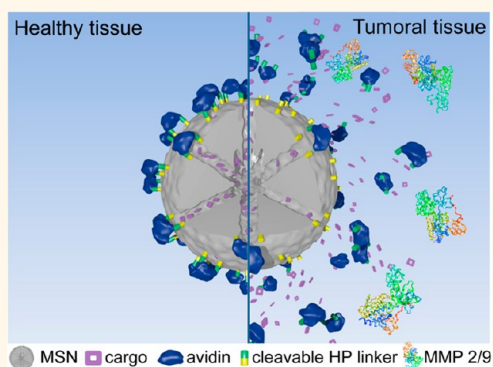


Protease-Mediated Release of Chemotherapeutics from Mesoporous Silica Nanoparticles to *ex Vivo* Human and Mouse Lung Tumors

Sabine H. van Rijt,^{*,†} Deniz A. Bölükbas,^{†,||} Christian Argyo,^{*,||} Stefan Datz,[‡] Michael Lindner,[§] Oliver Eickelberg,[†] Melanie Königshoff,[†] Thomas Bein,^{*,‡} and Silke Meiners[†]

[†]Comprehensive Pneumology Center (CPC), University Hospital, and [§]Center of Thoracic Surgery Munich, Asklepios Clinic Munich-Gauting, and Asklepios Biobank for Diseases of the Lung, Comprehensive Pneumology Center (CPC), Ludwig-Maximilians University and Helmholtz Zentrum München, Member of the German Center for Lung Research (DZL), Max-Lebsche-Platz 31, 81377, Munich, Germany and [‡]Department of Chemistry and Center for NanoScience (CeNS), University of Munich (LMU), Butenandtstrasse 5-13(E), 81377 Munich, Germany. ^{||}D. Bölükbas and C. Argyo contributed equally to this work.

ABSTRACT Nanoparticles allow for controlled and targeted drug delivery to diseased tissues and therefore bypass systemic side effects. Spatiotemporal control of drug release can be achieved by nanocarriers that respond to elevated levels of disease-specific enzymes. For example, matrix metalloproteinase 9 (MMP9) is overexpressed in tumors, is known to enhance the metastatic potency of malignant cells, and has been associated with poor prognosis of lung cancer. Here, we report the synthesis of mesoporous silica nanoparticles (MSNs) tightly capped by avidin molecules *via* MMP9 sequence-specific linkers to allow for site-selective drug delivery in high-expressing MMP9 tumor areas. We provide proof-of-concept evidence for successful MMP9-triggered drug release from MSNs in human tumor cells and in mouse and human lung tumors using the novel technology of *ex vivo* 3D lung tissue cultures. This technique allows for translational testing of drug delivery strategies in diseased mouse and human tissue. Using this method we show MMP9-mediated release of cisplatin, which induced apoptotic cell death only in lung tumor regions of *Kras* mutant mice, without causing toxicity in tumor-free areas or in healthy mice. The MMP9-responsive nanoparticles also allowed for effective combinatorial drug delivery of cisplatin and proteasome inhibitor bortezomib, which had a synergistic effect on the (therapeutic) efficiency. Importantly, we demonstrate the feasibility of MMP9-controlled drug release in human lung tumors.



KEYWORDS: mesoporous silica nanoparticles · controlled drug delivery · cisplatin · lung cancer · combination treatment · bortezomib · matrix metalloproteinase-9 · *ex vivo* 3D lung tissue cultures · nanomedicine

In the past decade, the use of nanoparticles as inert carriers for therapeutics has revolutionized the field of drug delivery. Such nanocarrier systems have shown advantageous features resulting in improved accumulation of active drugs at disease sites and have contributed to reduced systemic toxicity.¹ However, release systems of many drug carriers rely on spontaneous degradation of the nanoparticle *in vivo* (*e.g.*, hydrolysis) and do not allow for controlled drug release. Controlled drug delivery can be achieved by exploiting the (patho)physiologic characteristics of biological microenvironments, such as reducing conditions, changes of pH (*e.g.*, acidic endosomal

compartments), or altered levels of disease-specific enzymes. For example, matrix metalloproteinases 2 and 9 (MMP2 and MMP9) are overexpressed in advanced stages of cancer including lung cancer, whereas they are minimally expressed in healthy tissue.² Indeed, elevated levels of MMP9 in the tumor microenvironment enhance the metastatic potency of malignant cells and correlate with tumor progression, angiogenesis, or metastasis.³ In particular, increased expression of MMP9 has been associated with poor prognosis of lung cancer.^{4,5} Specific peptide sequences can be exploited as protease-sensitive linkers⁶ to allow for controlled release of chemotherapeutics from

* Address correspondence to sabine.vanrijt@helmholtz-muenchen.de, bein@lmu.de.

Received for review February 25, 2014 and accepted February 21, 2015.

Published online February 22, 2015
10.1021/nn5070343

© 2015 American Chemical Society

nanoparticles, as recently shown by the use of MMP2/9-sensitive peptides for drug delivery.^{7–13} Consequently, the use of MMP2/9-responsive nanoparticles represents a promising strategy for local treatment of aggressive lung cancer.

Multifunctional mesoporous silica nanoparticles (MSNs) are attractive carriers for drug delivery.¹⁴ They offer unique properties such as tunable pore sizes and pore volumes for high drug loading capacity and efficient encapsulation of a wide variety of cargo molecules.¹⁵ Additionally, these carriers can be selectively functionalized at specific sites within the nanoparticle.¹⁶ For example, an outer-shell functionalization enables the attachment of external functions exclusively on the outer surface of the particle, which do not interfere with the pore environment. This can be exploited to create stimuli-responsive pore sealing for controlled drug release.^{17–21} For example, MSN pore closing can be achieved by utilizing biotin–avidin complexation, which serves as a bulky biomolecule-based valve blocking the entrances of the MSN pores.²²

In this work, we developed avidin-capped MSNs functionalized with linkers that are specifically cleaved by MMP9, thereby allowing for controlled release of chemotherapeutics from the MSNs in high MMP9-expressing lung tumor areas. We demonstrate efficient protease sequence-specific release of the incorporated chemotherapeutic cisplatin (CP), as well as combination treatment with the proteasome inhibitor bortezomib (Bz) in two lung cancer cell lines. To assay therapeutic effectiveness in diseased tissue, we established a novel experimental setup using 3D lung tissue cultures (3D-LTCs). This technique allows for spatio-temporal resolution and quantification of nanoparticle-mediated drug delivery in the preserved 3D environment of diseased mouse and human lung tissue. We here demonstrate MMP9-mediated tumor-site-selective drug release and tumor cell death in mouse and human lung tumors revealing the feasibility of MMP9-controlled drug site-selective delivery for the treatment of lung cancer.

RESULTS

Synthesis and Characterization of MMP9-Responsive MSNs.

According to previous reports, the MSNs were synthesized by a sol–gel procedure.^{16,23} In the present work, the external surface of the MSNs was coated with a heptapeptide (HP) linker (MSN_{HP}) consisting of a biotin functionality on the periphery (for detailed synthesis procedure, refer to the SI). This HP sequence is selectively recognized by MMP9 for proteolysis (RSWM**GLP**, cutting sequence shown in bold).²⁴ As a negative control, MSNs containing a noncleavable heptapeptide (NHP) attached to the outer surface of the particles were synthesized (MSN_{NHP}). In this NHP-biotin linker, the specific cleavage site for MMP9 is lost due to an exchange of a single amino acid (RSW**L**LLP, exchanged

amino acid shown in bold). After dye/drug uptake into the mesopores of both particle types, the glycoprotein avidin (66 kDa, av diameter ~8 nm) was attached to the outer surface of the particles *via* noncovalent linkage to the biotin groups. The particles have been termed throughout the text as cMSN (MMP9 cleavable linkers) or ncMSN (MMP9 noncleavable linkers). Avidin shows high affinity to biotin and therefore acts as a bulky gatekeeper to block the mesopores of the silica nanoparticles. The complete synthesis strategy and characterization of the particles are depicted in Figure 1. Comprehensive characterization of the synthesized MSNs involved a range of physicochemical methods – thermogravimetric analysis, zeta potential, dynamic light scattering, nitrogen sorption, and infrared (IR) spectroscopy (Figure 1B–F, respectively) – all of which confirmed the successful synthesis of cMSN or ncMSN. See also Table 1, Figure S1, and the SI for additional information. From these data, we conclude that the attachment of the avidin gatekeepers *via* short heptapeptide-biotin linkers (cleavable and noncleavable for MMP9) to the external surface of MSNs was successful. In order to prove the MMP9-specific release behavior of our nanoparticle system, release experiments with fluorescein were performed as previously reported.²² Only upon the addition of recombinant MMP9 to the particle suspension an increase in fluorescence intensity over time was observed, reaching a plateau after about 16 h. Importantly, no release of the preloaded fluorescein was observed for MSNs containing a noncleavable heptapeptide linker (ncMSN) (Figure 1G). Furthermore, MMP2 was also able to induce fluorescein release from the particles, but with slower kinetics, compared to MMP9 (Figure S1D). This is not surprising, as MMP2 has different enzyme kinetics compared to MMP9 and has been shown to degrade several substrates that are not degraded by MMP9 and *vice versa*.²⁵ For this reason, we chose to continue with MMP9 in the *in vitro* studies. However, it is important to note that both enzymes are overexpressed in lung cancer, and so we expect a cumulative effect on cargo release *in vivo*.^{4,5} The cMSN particles took up the drug cisplatin very efficiently (0.44 ± 0.02 mg/mg cMSN, Table S1) and showed specific release of cisplatin when incubated with recombinant MMP9, whereas no release of cisplatin could be detected in the absence of MMP9 (Table S1). Furthermore, the avidin-capped particles preloaded with fluorescein (cMSN-fluorescence) showed stability of the capping system for up to 16 h (Figure S1F). Colloidal stability of our particles was retained for up to 7 days (168 h), after which time agglomeration of the MSNs could be observed in solution (Figure S1G). In addition, long-term cargo release experiments of fluorescein-loaded cMSN in HBSS buffer solution (no MMP9) showed that the particles were stable for at least 28 days (Figure S1H), similar to what we previously observed for related MSNs with organic coatings.^{26,27} Consequently, the

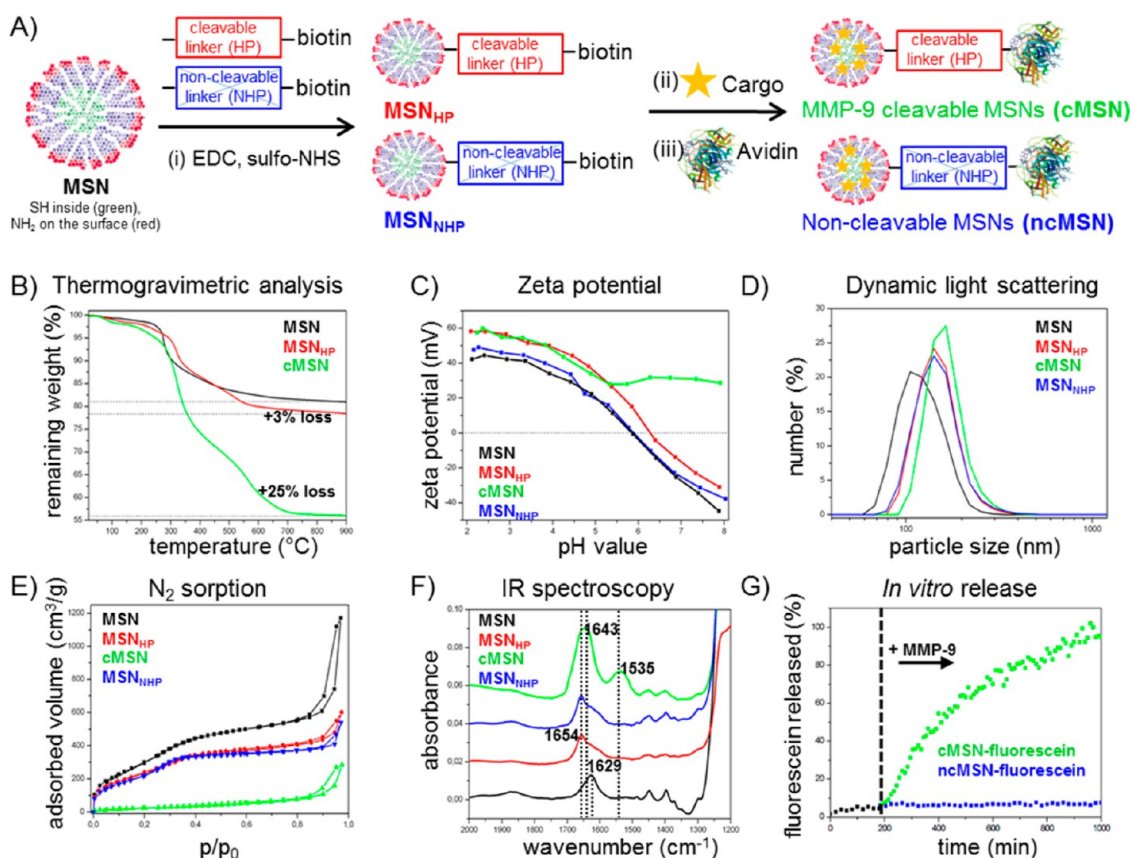


Figure 1. Synthesis and characterization of MMP9-responsive mesoporous silica nanoparticles (MSNs). (A) Synthesis scheme of core (green, thiol groups), shell (red, amino groups) functionalized MSNs. (i) EDC amidation of amino groups with carboxy groups of the MMP9 cleavable HP (HP, red) or the MMP9 noncleavable HP-biotin linker (NHP, blue) results in a covalent attachment to the external particle surface (MSN_{HP} , MSN_{NHP}). (ii) After cargo incorporation (cisplatin (CP) or bortezomib combination treatment (CT), yellow star), (iii) the strong binding affinity of biotin to avidin leads to blocking of the mesopores of MSNs with MMP9 cleavable linkers (cMSN) and MMP9 noncleavable linkers (ncMSN). Characterization of MSNs. (B) Thermogravimetric analysis, (C) zeta potential measurements, (D) dynamic light scattering, (E) nitrogen sorption isotherms, and (F) infrared spectroscopy (all curves are shifted by a value of 0.02 along the y-axis for clarity) of MSN (black), MSN_{HP} (red), MSN_{NHP} (blue), and cMSNs (green). (G) Release kinetics of fluorescein from cMSNs and ncMSNs before and after addition of MMP9.

TABLE 1. Structural Parameters of Functionalized MSNs

Sample	Particle size ^a (nm)	BET surface area (m ² /g)	Pore volume ^b (cm ³ /g)	DFT pore size ^c (nm)
MSN	106 ± 9	1150	0.67	3.6 ± 0.1
MSN_{HP}	142 ± 13	882	0.55	3.6 ± 0.1
cMSN	164 ± 15	90	0.05	- ± 0
MSN_{NHP}	142 ± 17	825	0.52	3.6 ± 0.1

^a Particle size refers to the peak value of the size distribution derived from DLS measurements. ^b Pore volume was calculated up to a pore size of 8 nm to remove the contribution of interparticle textural porosity. ^c DFT pore size refers to the peak value of the pore size distribution.

above experiments validate highly specific release behavior of fluorescein and cisplatin from cMSNs by recombinant MMP2/9 enzymes.

MMP9-Responsive Release of Cargo to Lung Cancer Cells. We next investigated MMP9-mediated release of the chemotherapeutic drug cisplatin in two human lung cancer cell lines (A549 and H1299) as a function of cell viability. MMP9-dose-responsive release of cisplatin from the nanoparticles and subsequent induction of

dose-dependent cell death were observed in both cell lines (Figure 2A and B).

It is important to note that the MSNs were pre-loaded by diffusing a defined cisplatin solution into the particles, after which the particles were sealed and washed. In the figures, these loading concentrations are referred to as loaded cisplatin concentrations. However, the amount of cisplatin released from the particles, thus the effective cisplatin concentration the

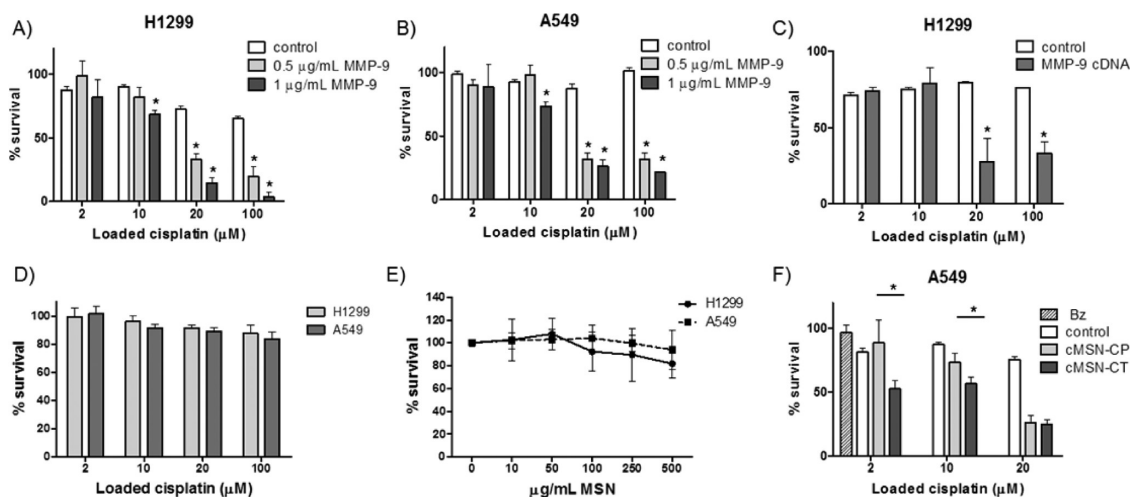


Figure 2. MMP9-responsive release in lung cancer cells. Controlled release of cisplatin (CP) from cMSN as measured by percent cell survival after 24 h exposure, incubated with 0 (white bars), 0.5 (light gray bars), or 1 $\mu\text{g}/\text{mL}$ (dark gray bars) MMP9 in H1299 (A) and A549 cells (B) or (C) with MMP9 cDNA (gray bars) or empty vector transfected cells (white bars) in H1299. (D) ncMSN particles encapsulating CP incubated in the presence of 1 $\mu\text{g}/\text{mL}$ MMP9 for 24 h did not result in significant cytotoxicity in H1299 (light gray bars) and A549 cells (dark gray bars). (E) Cytotoxicity of cMSNs determined by WST-1 assay in H1299 and A549 lung cancer cell lines after 24 h of exposure. (F) Controlled release of cMSNs loaded with CP alone (light gray bars) and in combination with 1 μM bortezomib (CT, dark gray bars) in MMP9 cDNA transfected A549 cells, in comparison to empty vector transfected A549 cells (white bars). Untreated cells were set to 100% survival; * means a significant decrease in percent cell survival compared to control ($p < 0.05$). Values given are an average of three independent experiments \pm SD.

cells or tissue were exposed to, was much lower, as the incorporated amount is lower than the provided amount in the stock solution. Of note, we observed a high cisplatin MSN loading of $440 \pm 0.02 \mu\text{g}/\text{mg}$ MSN, when diffusing 10 mM cisplatin stock solution into the pores (Table S1). The cisplatin concentration released from the particles was estimated to be an order of 10-fold less (then the used stock solution) when compared to free cisplatin as determined by a dose–response viability curve of direct cisplatin treatment in A549 and H1299 cells (Figure S2A).

To determine if cell-secreted MMP9 was able to open the particle caps, A549 and H1299 cells were transiently transfected with MMP9 cDNA and overexpression of active MMP9 was validated with gelatin zymography (Figure S2B). MMP9-overexpressing cells responded to cisplatin-loaded MSNs with pronounced loss of cell viability compared to empty vector transfected control cells. This demonstrates that the cell-secreted concentrations of MMP9 were able to trigger the release of chemotherapeutic drugs from stimuli-responsive MSNs (Figure 2C). Importantly, cisplatin-loaded MSNs containing noncleavable linkers (ncMSN-CP) did not induce any cell death in either cell line (Figure 2D), indicating tight sealing of the particles. Importantly, nonloaded MSNs were found to be nontoxic at the dose applied (50 $\mu\text{g}/\text{mL}$) (Figure 2E).

Because MSNs can efficiently encapsulate multiple drugs, these carriers offer a unique opportunity for combinatorial drug delivery, which overcomes the problem of acquired drug resistance.²⁸ Proteasome inhibitors are promising combinatorial drugs, as suggested by multiple clinical trials, since they effectively

inhibit proliferation of tumor cells, sensitize them to apoptosis, and overcome drug resistance.²⁹ Bortezomib is FDA-approved for the treatment of multiple myeloma and mantle cell lymphoma and is currently being tested in phase II clinical trials for lung cancer.³⁰ In our setup, nanoparticles loaded with nontoxic doses of cisplatin and Bz when used on their own, induced significant cell death in the presence of MMP9 when applied in combination (Figure 2F). Augmented cytotoxicity was largest for the lowest cisplatin dose (2 μM), with an increased cytotoxicity of over 35% in the presence of Bz. This was a remarkable 5- to 10-fold increase in cytotoxic potency for nontoxic doses of a single drug. Cells exposed to MSNs loaded with cisplatin and Bz (cMSN-CT) in the absence of MMP9 showed no significant loss in cell viability (Figure 2F, white bars), indicating again tight sealing of the particles. These results demonstrated that the combinatorial delivery of cisplatin and Bz *via* nanoparticles induced an additive cytotoxic effect and thus allow for a reduction of drug doses.

Application of 3D Mouse and Human Lung Tissue Cultures.

Having shown the feasibility of MMP9-mediated drug release from the avidin-capped MSNs in lung tumor cell lines, we next aimed to validate MMP9-responsive drug release in the complex setting of lung tumor tissue. For that purpose, we made use of a novel 3D *ex vivo* tissue culture method. This technology involves the preparation of *ex vivo* tissue cultures from healthy and tumoral mouse and human lungs, which can be cultured for up to 7 days (Figure 3A) (Uhl *et al.* unpublished). For our purposes, mouse and human lung tissue slices of 200 μm thickness were exposed for

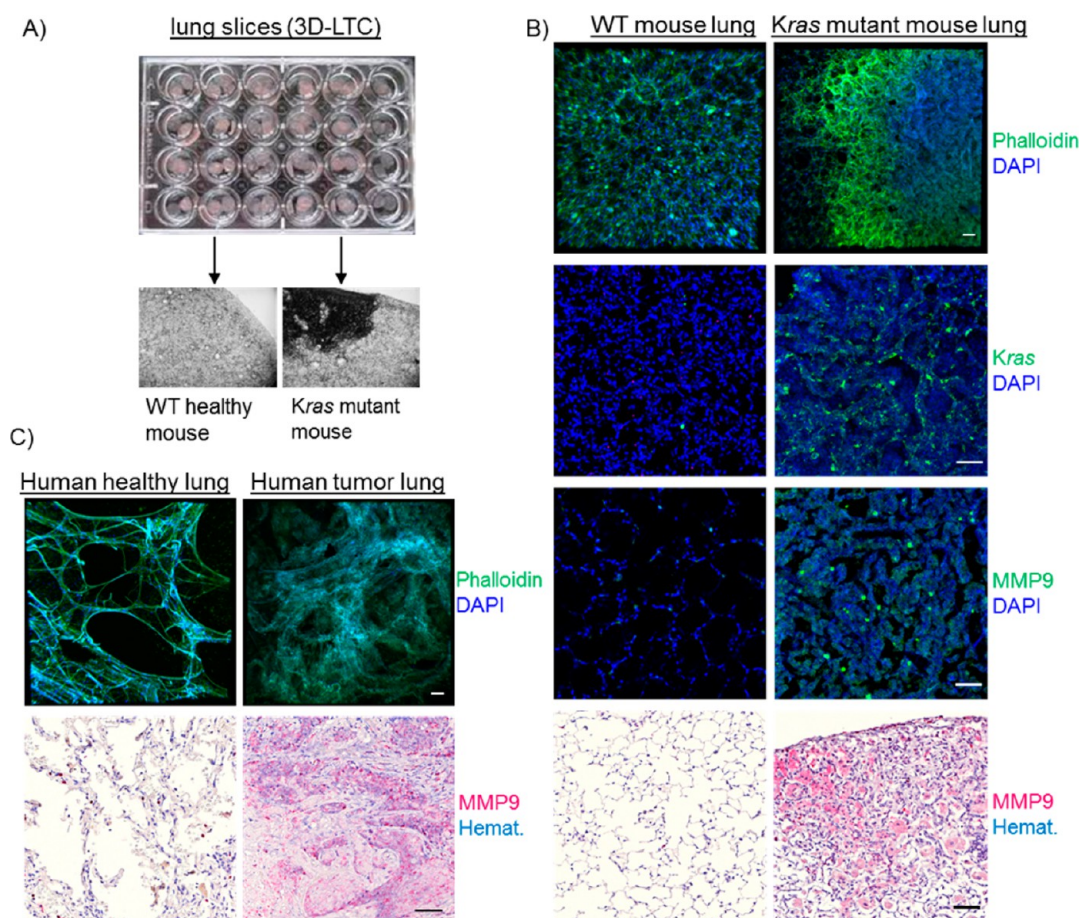


Figure 3. 3D human and mouse *ex vivo* tissue culture (3D-LTC). (A) 200 μm thick WT and *Kras* mouse lung tissue slices were kept under normal culture conditions. *Kras* mouse tumors can be easily observed with bright-field microscopy (5 \times objective). (B) Confocal microscopy images of WT mouse and *Kras* mutant mouse 3D-LTC with (from top to bottom) phalloidin, *Kras*, and MMP9 staining using immunofluorescence and immunohistochemistry. (C) 3D images of tumorous and tumor-free lung tissues from human with (from top to bottom) phalloidin and MMP9 staining using immunohistochemistry (Hemat. = hematoxylin). The scale bar is 50 μm .

24 to 72 h to MSNs that had been covalently labeled with Atto633 in their core. After treatment, lung tissue slices were fixed and stained using immunofluorescence (Figure 3B). As a model for murine lung tumors, we used transgenic mice carrying a spontaneously activated *Kras* mutation, which are highly predisposed to a range of tumor types, however predominantly show early spontaneous development of lung cancer after only a few weeks of age.³¹ This mouse model not only carries the most common mutation, *i.e.*, *Kras*, observed in human lung cancer patients^{32–34} but also closely resembles spontaneous tumor development *via* oncogene activation as seen in humans. Human material was obtained from freshly excised lung tumor tissue from consenting patients. Tumor lesions were clearly detectable in both mouse *Kras* and human patient derived 3D-LTC, as characterized by loss of parenchymal lung structure and the appearance of dense cell populations (Figure 3B and 3C, phalloidin staining). Staining of 3D-LTCs with a *Kras* antibody confirmed its overexpression in *Kras* tumor and non-tumor mouse tissue, compared to low expression in

3D-LTC of wild-type (WT) mice (Figure 3B and Figure S4A). MSNs suspended in culture media distributed evenly and reproducibly in the tissue (Figure S4B). Nonloaded particles were not toxic to the 3D-LTC for up to 72 h of exposure, as revealed by the absence of apoptotic caspase-3 activation (Figure S4C). High MMP9 expression was detected in tumor lesions of *Kras* mutant mice and in tumorous human tissue by MMP9 immunofluorescence staining (Figures 3B,C and S4D) and by immunohistochemistry of paraffin-embedded lung tissue (Figures 3B,C and S4E). MMP9 expression was highest in early phase neoplasms, and staining was most pronounced at the invading peripheries of the tumors (Figure S4D). These data confirm MMP9 overexpression in *Kras* mouse and human lung tumors, validating this model as suitable for MMP9-mediated drug delivery.

MSN-Mediated MMP9-Responsive Drug Delivery to *Kras* Mutant Mouse Lungs. Having established the 3D-LTCs of *Kras* mouse lung tumor tissue as a powerful tool for MMP9-mediated drug delivery *via* nanoparticles, we next evaluated therapeutic effectiveness of drug

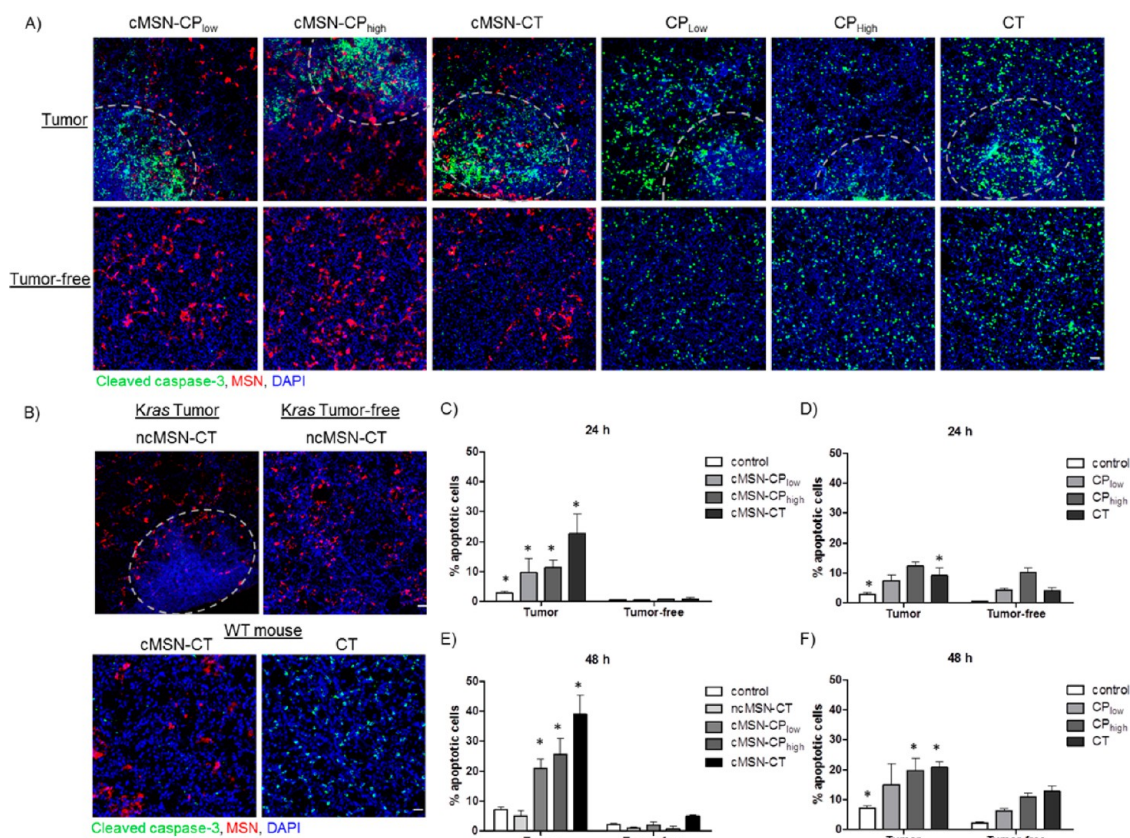


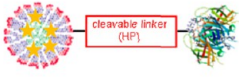
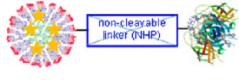

Figure 4. Therapeutic efficacy of MMP9-responsive MSNs in *Kras* mutant mouse lungs. (A) *Kras* mutant mouse 3D-LTC exposed to MSNs encapsulating either a low dose of CP (cMSN-CP_{low}), high dose of CP (cMSN-CP_{high}), low dose of CP in combination with Bz (cMSN-CT), or comparable doses of the free drugs (CP/CT) for 48 h. (B) *Kras* mouse 3D-LTC exposed to MSNs with noncleavable linkers encapsulating combination treatment (ncMSN-CT) for 48 h (upper panel) and WT mouse 3D-LTC exposed to MSNs with MMP9-cleavable linkers encapsulating combination treatment (cMSN-CT) or free (nonencapsulated) drugs (CT) for 48 h (lower panel). The scale bar is 50 μm . Comparable sized tumors were chosen for microscopy (indicated by dotted line); tumor-free refers to images that were made in a nontumor area of a *Kras* 3D-LTC. Nuclear staining (DAPI) is shown in blue, apoptotic marker (cleaved caspase-3 positive) in green, and Atto633-labeled MSNs in red. Images shown are representative for three independent experiments (see also Figures S6, S7). Quantification of apoptotic cells (cleaved caspase-3) per number of counted nuclei (DAPI) in tumor and tumor-free areas in *Kras* 3D-LTC after (C, D) 24 h of exposure and (E, F) 48 h of exposure to MSNs encapsulating drugs (cMSN-CP/CT) or free (nonencapsulated) drugs (CP/CT), respectively. Nontreated control slices (white bars) and control MSNs (*i.e.*, ncMSN-CT) (light gray bar, 48 h exposure) were also included in the study. * means a significant increase in apoptosis compared to a nontumor control area ($p < 0.05$). Values given are average of three independent experiments \pm SD (see also Figures S7, S8).

release from our functionalized nanoparticles (cMSN). For that, lung tissue slices of *Kras* mutant mice were exposed to particles that contained different concentrations of cisplatin (cMSN-CP_{low} and cMSN-CP_{high}; 5 \times higher concentration) or a combination of low doses of cisplatin with bortezomib (cMSN-CT) for 24 or 48 h. We established the dose by exposing the lung tissue slices to various concentrations of cisplatin. At the reported cisplatin concentrations (Table 2) we observed a significant amount of apoptosis of approximately 12% of cells after 24 h and 20% after 48 h using the higher dose of cisplatin (Figure 4D,F), as indicated by a significant amount of caspase-3 positive staining (Figure 4A right panel and Figures S6A,B and S7A,B). On the basis of our *in vitro* findings of about 10-fold less encapsulation of cisplatin into the MSNs, we encapsulated 10 \times higher doses of cisplatin solution inside the MSNs to be able to achieve a similar effect and applied those to the lung slices (see Table 2 for an overview of

used doses). Importantly, a similar induction of tumor cell death was observed for both the encapsulated drugs and the drugs alone for all tested doses and time points, showing that the chosen doses were effective and comparable to each other (Figure 4C–F).

Strikingly, all nanoparticles containing chemotherapeutic(s) induced apoptosis only in tumor lesions of *Kras* lungs, while not affecting tumor-free regions in the same *Kras* lung tissues (Figure 4A). In addition, we observed a dose-dependent therapeutic effect on apoptotic cell death, with the combination therapy (cMSN-CT) being most effective (Figure 4A). In contrast, *Kras* mutant mouse 3D-LTC exposed to comparable doses of free (nonencapsulated) drug(s) (CP or CT) resulted in apoptotic cell death that did not discriminate much between tumorous and nontumorous tissue (Figure 4A). Of note, MSNs with noncleavable linkers encapsulating both drugs (ncMSN-CT) did not cause any significant apoptotic cell death in *Kras*

TABLE 2. Drug Doses Used for the Mouse Lung Tissue Slices Experiments

As represented in Fig. 1	Label	(loaded) drug concentrations
	cMSN-CP _{low} cMSN-CP _{high} cMSN-CT	2 mM cisplatin 10 mM cisplatin 2 mM cisplatin + 1 μ M Bortezomib
	ncMSN-CP _{low} ncMSN-CP _{high} ncMSN-CT	2 mM cisplatin 10 mM cisplatin 2 mM cisplatin + 1 μ M Bortezomib
	CP _{low} CP _{high} CT	0.2 mM cisplatin 1 mM cisplatin 0.2 mM cisplatin + 0.2 μ M Bortezomib

tumors or in healthy tissue in *Kras* lungs (Figure 4B upper panel). In addition, healthy lungs of WT mice exposed to drug-loaded nanoparticles (cMSN-CT) did not show significant signs of apoptosis, whereas exposure to comparable doses of free (nonencapsulated) drugs caused apoptotic cell death that distributed evenly in the healthy tissue (Figure 4B and Figure S5), further proving the selective cytotoxic effect of our MSNs. The dose- and time- dependent therapeutic effects of the MSNs were quantified by counting the number of apoptotic cells *versus* the total number of cells in lung tissue slices containing tumors of comparable size (see Figures S6 and S7 for the images used for quantification). Of note, cell death in the tumor area was 10- to 25-fold higher compared to the nontumor area upon nanoparticle-mediated drug delivery. This was even more pronounced after 48 h (Figure 4E). The effect was highest for the combination therapy with a 25-fold increase in apoptotic tumor cell death, while exposure of *Kras* lung tissue to Bz alone did not cause any significant apoptosis (Figure S8A). In contrast to the nanoparticle-mediated drug delivery, *Kras* lungs exposed to comparable doses of cisplatin \pm Bortezomib for 24 and 48 h showed a similar degree of apoptotic cell death in the tumor and nontumor areas (Figure 4D and F). Only for the highest doses (CP_{high} and CT) a small but significant increase in tumor cell death was observed. This might be attributed to the increased effectiveness of cisplatin toward fast-dividing and “leaky” tumor cells.³⁵

Importantly, MSNs induced apoptosis correlated with MMP9 expression in tumor lesions (Figures 5A and S8B). Detailed analysis of the 3D-LTC revealed that apoptosis took place throughout the tumor while the particles remained mainly on the top of the tissue, where they associated with the tissue (Figures 5B and S8C). This observation suggests that the particles are first immobilized on the tissue and subsequently cleaved by overexpressed MMP9 on the surface of the tissue, and the released chemotherapeutic(s) effectively diffuse into the tissue. A similar distribution of apoptotic cells in the tumor tissue was observed for 3D-LTC

exposed to the drug alone (Figures 5B and S8C). This indicates that deep penetration of nanoparticles into the tumor tissue is not required, as the released drugs effectively diffuse throughout the tissue. Moreover, we confirmed that the cytotoxic effects were mainly restricted to epithelial tumor cells by costaining of 3D-LTCs with cleaved caspase-3 and the epithelial cell type marker E-cadherin (Figures 5C and S8D). These data clearly demonstrate tumor-site-selective drug delivery by our nanoparticles.

MMP9-Responsive Drug Delivery to Human Lung Tumors. In a final step, we set out to assess protease-responsive drug delivery from our nanoparticles in human lung tumors. For that purpose, we used 3D-LTCs from freshly excised human lung cancer tissue obtained from different donors. Cisplatin-loaded nanoparticles (cMSN-CP_{low}) induced pronounced apoptotic cell death in human cancer tissue after 72 h of exposure. This correlated well with particle density on the tissue (Figure 6A). Furthermore, therapeutic effectiveness of the cMSN-CP was not dependent on the tumor type, as apoptotic cell death was induced in both metastatic and primary lung tumors (Figure 6A). Untreated control tissue showed only a minor degree of apoptosis, which might be attributed to the tissue-cutting procedure (Figure 6A). Human 3D-LTCs exposed to noncleavable MSNs (ncMSN-CP) did not show significantly more apoptosis compared to control tissues (Figure 6A, middle panel), confirming MMP9 sequence-specific drug release. Importantly, cMSN-CP_{low} particle exposure did not induce any apoptosis in healthy human tissue (Figure 6B). MSN-induced apoptosis was observed throughout the tumor tissue (Figure S9). The therapeutic effect of the particles was confirmed by quantification of cleaved caspase-3 levels by Western blot analysis using whole 3D-LTC homogenates (Figure 6C).

DISCUSSION AND CONCLUSIONS

Nanoparticles as drug delivery carriers have received a lot of attention in the last decades, and several formulations have been approved by the FDA and

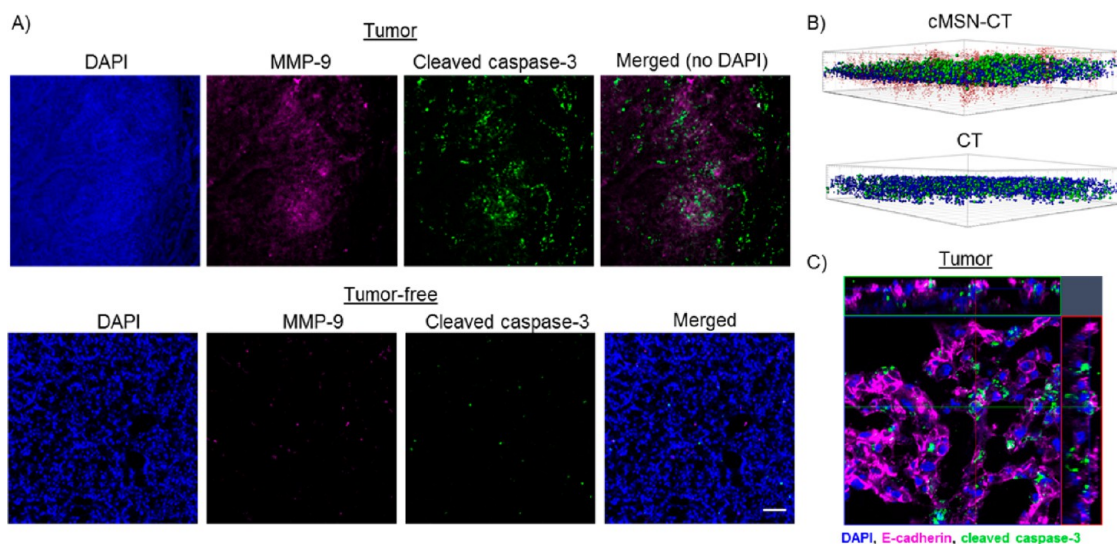


Figure 5. (A) *Kras* 3D-LTC exposed to cMSN-CT for 48 h with MMP9 antibody costaining (magenta, maximum intensity projections of the different channels, white dots in merged image show direct overlay) in tumor (top) and tumor-free (bottom) areas. (B) Exposed *Kras* 3D-LTC showing only the calculated number of particles, nuclei, and apoptotic cells per 3D-LTC tissue slice from the side where tumor tissue is located. Red spots represent the calculated particles, blue spots represent the nuclei, and green spots represent the apoptotic cells in cMSN-CT-exposed 3D-LTC (top panel) and CT-exposed 3D-LTC (bottom panel). Original stainings were omitted for clarity. (C) *Kras* 3D-LTC exposed to cMSN-CT for 48 h with E-cadherin antibody costaining (magenta, orthographic representation using a 63 \times objective). The nuclear staining (DAPI) is shown in blue; apoptotic marker (cleaved caspase-3) in green. The fluorescence signal originating from Atto 633-labeled MSN particles was omitted from the images for clarity (for A and C). Scale bar is 50 μ m.

European Medicines Agency for the treatment of cancer.³⁶ Many of these formulations offer improved pharmacodynamics over the free drug by increasing their bioavailability and tumor delivery efficiency. In addition, nanoparticles such as MSNs can be developed for inhalation therapy,³⁷ which is advantageous for the treatment of lung cancer, as drugs are directly administered in the target organ, bypassing the gastrointestinal tract and the liver, and problems associated with stability throughout blood circulation become irrelevant. Indeed, our preliminary data indicate that the particles are well distributed in the lungs and have low lung toxicity. The drug release of nanocarriers such as liposomes and polymers is sustained (*i.e.*, slow release of drugs over time that is not controllable). A promising approach to further increase the tumor specificity and effectiveness of nanoparticles is the ability to release high concentrations of drugs only in the extracellular matrix in close proximity to the tumor site. Cancer-specific extracellular enzymes can be used to achieve this goal. For example, MMP9 is overexpressed in lung tumors, known to enhance the metastatic potency of malignant cells, and is associated with poor prognosis in lung cancer.^{2–5} The feasibility and promise of MMP2/9-responsive drug therapy has previously been demonstrated in *in vivo* mouse xenografts of the pancreas,³⁸ fibrosarcoma,¹¹ glioblastoma (brain),¹² and hepatoma (liver),³⁹ demonstrating that this is a promising technology for treatment of a variety of cancers. No such *in vivo* data for non-small-cell lung cancer (NSCLC) currently exist.

In the present study, we report the synthesis of novel mesoporous silica nanoparticles containing an MMP9-responsive avidin capping system. MMP-responsive MSNs were reported only in three studies recently, by Singh *et al.*,⁴⁰ Zhang *et al.*,⁴¹ and Xu *et al.*⁴² However, these studies did not report a MMP9 sequence-specific capping system for controlled drug delivery from the MSNs. In the study by Singh *et al.*, the MSNs were coated with a polymer shell consisting of MMP substrate polypeptides with a degradable sequence. In the study by Zhang *et al.*, MSNs were coated with a polyanion layer, preventing particle uptake by healthy cells, which could be removed *via* MMP cleavage in MMP2-expressing colon and squamous cancer cell lines. After (tumor) cell uptake of the particle, cargo release (doxorubicin) was obtained by a redox-driven release mechanism. In another study by Xu *et al.*, gelatin was used both as a gatekeeper and as a degradable substrate for MMPs in gelatin-coated MSNs and showed efficacy in a MMP2-overexpressing colon cancer cell line and a xenograft mouse model. Nevertheless, the efficiency of pore sealing to prevent unwanted drug release was poor in this system. In contrast, here we show effective MMP2/9 sequence-specific release of loaded cargo from the biomolecule-capped MSN system in two non-small-cell lung cancer cell lines and in mouse and human lungs. To achieve this, we developed a novel *ex vivo* tissue culture application (3D-LTC) to test our particles. The 3D-LTC technique allows for high-resolution and spatiotemporal imaging of the therapeutic effect of nanoparticles in selected areas of interest (*e.g.*, diseased *versus* healthy areas) within

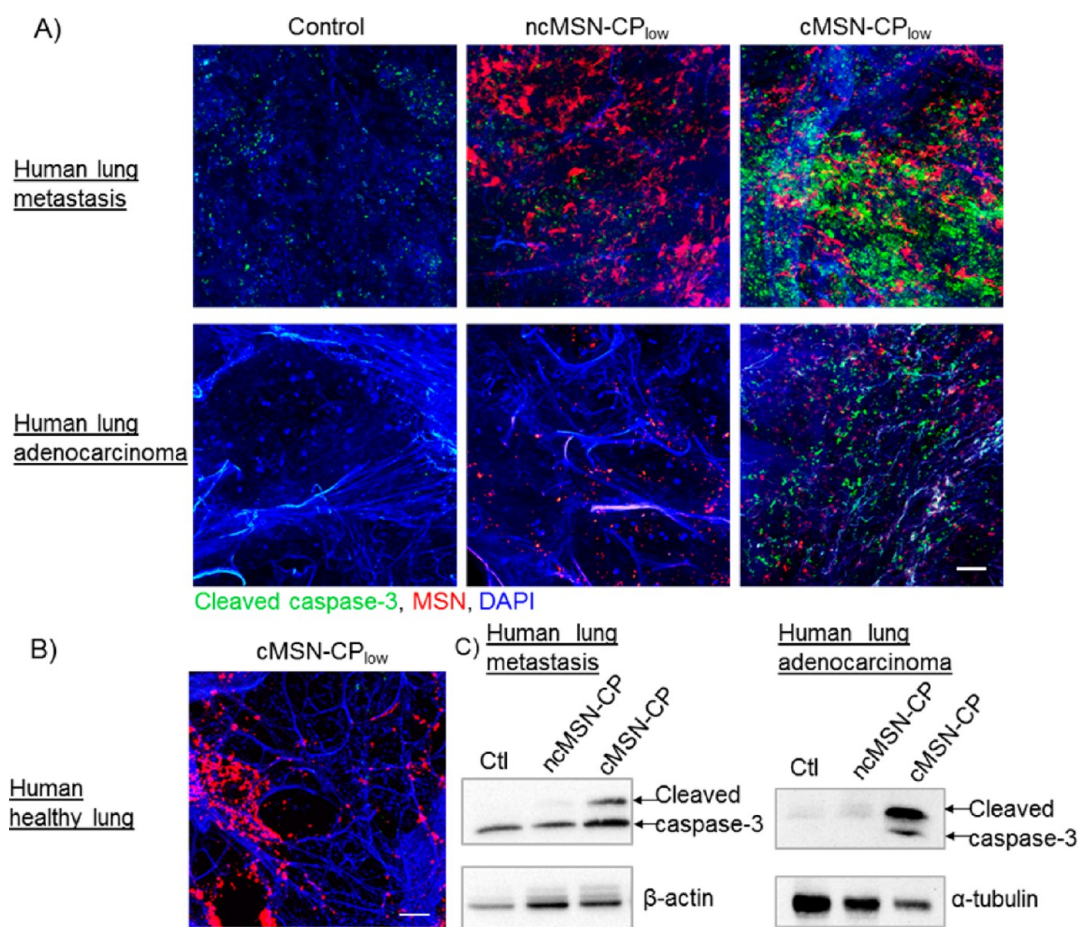


Figure 6. Therapeutic effect of MMP9-responsive MSNs in human lungs. (A) Human lung adenocarcinoma and (B) human healthy lung 3D-LTC exposed to cMSN-CP_{low} or ncMSN-CP_{low} for 72 h. Nonexposed control slices were included in the study. Nuclear staining (DAPI, blue), cleaved caspase-3 (green), and MSNs (red). The scale bar is 50 μ m. Images shown are representative for three different sections within the tumor (see also Figure S9). (C) Western blot analysis of human 3D-LTC exposed to cMSN-CP_{low} and ncMSN-CP_{low} for 72 h.

the complex 3D structure of lung (cancer) tissue. While previous reports have used 3D-LTC predominantly for short-term toxicological analysis of nanoparticles,^{43–45} we studied the therapeutic effect of nanoparticles in relevant disease models. As a model for murine lung tumors, we used transgenic mice carrying a spontaneously activated *Kras* mutation, which show early spontaneous development of lung cancer after only a few weeks of age. As this model closely reflects the human pathophysiology, we believe that therapeutic strategies that are confirmed in this model are more likely to translate to humans than the commonly used xenograft mouse models. Furthermore, finding therapeutic strategies that work against *Kras* tumors is promising, as *Kras* mutations result in aggressive cancers, are generally correlated with poor prognosis, and are associated with reduced responsiveness to many existing therapies.^{46–48} Additionally, this technique allowed us to confirm our findings also in diseased human tissue, which represents a major advance in closing the gap between drug development and application in the clinic. Using this method, we show that *in vivo* MMP9 concentrations are locally highly

expressed in mouse *Kras* tumor and in patient-derived explanted tumor tissue compared to healthy mouse and human lung tissue. Because MMP9 expression has been reported as a clinical marker for tumor progression and metastasis,⁴⁹ it is possible that these highly MMP9 positive tumor areas represent metastasis-prone tumor cells. A link between MMP9 expression and metastasis was also shown in mice, where MMP9-deficient mice had a reduced number of metastatic colonies.⁵⁰ MMP9-mediated drug delivery may thus most likely target metastatic tumor cell areas and therefore may effectively reduce tumor invasion and metastasis. Indeed, only MMP9-expressing *Kras* tumor areas were affected by MSN treatment, as revealed by spatiotemporal high-resolution imaging, whereas healthy lungs from WT mice and healthy areas in tumor-bearing mouse lungs remained unaffected. In contrast, slices exposed to free (nonencapsulated) drugs had an even distribution of apoptosis in tumor, tumor-free, and healthy lung tissue. Accordingly, quantification of the therapeutic effect showed that the MSNs were 10- to 25-fold more effective in tumor tissue, whereas the free drug was less than 2-fold more

effective in tumor tissue compared to the tumor-free areas in the same tissue slices. Furthermore, our 3D-LTC data proved the synergistic effect of our combinatorial drug delivery strategy and agrees very well with our *in vitro* data, where we observed a 5–10-fold increase in cytotoxic potency upon combinatorial drug delivery. Using proteasome inhibitors in combination with a commonly used chemotherapeutic is a novel approach for treatment of cancer in general and for lung cancer in particular. A phase II clinical trial study with bortezomib in combination with carboplatin (another platinum-based chemotherapeutic) showed promising progression-free and improved overall survival rates for treatment of NSCLC.⁵¹ Our report is the first in which nanoparticle-based controlled release of a proteasome inhibitor in combination with cisplatin shows greatly enhanced antitumor activity. Finally, we provide proof that these particles are also effective in human metastasis and adenocarcinoma lung cancer.

METHODS

Materials. Tetraethyl orthosilicate (TEOS, Fluka, > 98%), triethanolamine (TEA, Aldrich, 98%), cetyltrimethylammonium chloride (CTAC, Fluka, 25% in H₂O), mercaptopropyl triethoxysilane (MPTES, Fluka, > 80%), aminopropyl triethoxysilane (APTES, Sigma-Aldrich, 99%), ammonium fluoride (NH₄F, Fluka), ammonium nitrate (NH₄NO₃, Fluka), hydrochloric acid (HCl, 37%), Bio-PLGMWSR (HP-biotin, GenScript, 96.3%), Bio-PLLMWSR (NHP-biotin, GenScript, 90.1%), *N*-(3-(dimethylamino)propyl)-*N*'-ethylcarbodiimide hydrochloride (EDC, Aldrich), *N*-hydroxysulfosuccinimide sodium salt (sulfoNHS, Aldrich), avidin, egg white (Merck, Calbiochem), fluorescein disodium salt dihydrate (Acros), calcein acetoxymethyl ester (calcein-AM, Sigma-Aldrich), cisplatin (Sigma-Aldrich), bortezomib (Bz, Velcade, Millennium Pharmaceuticals), cleaved caspase-3 antibody (Asp175) (Cell Signaling, 9661), E-cadherin antibody (BD Biosciences, 610181), *Kras* antibody (Santa Cruz, SC30), MMP9 antibody (Millipore, AB19016), β -actin antibody (Cell Signaling), α -tubulin (Genetex), and secondary Alexafluor antibodies (Invitrogen) were used as received. Ethanol (EtOH, Aldrich, absolute), dimethyl sulfoxide (DMSO, Aldrich), and HBSS buffer (Gibco) were used as solvents without further purification. Bidistilled water was obtained from a Millipore system (Milli-Q Academic A10).

Synthesis Procedures. Particle synthesis of MSNs containing SH groups in the core particle and NH₂ groups on the particle surface (MSN) was performed. A mixture of TEOS (1.63 g, 7.82 mmol), MPTES (112 mg, 0.48 mmol), and TEA (14.3 g, 95.6 mmol) was heated under static conditions at 90 °C for 20 min in a polypropylene reactor. Then, a solution of CTAC (2.41 mL, 1.83 mmol, 25 wt % in H₂O) and NH₄F (100 mg, 2.70 mmol) in H₂O (21.7 g, 1.21 mmol) was preheated to 60 °C and rapidly added to the TEOS solution. The reaction mixture was stirred vigorously (700 rpm) for 20 min while cooling to room temperature. Subsequently, TEOS (138.2 mg, 0.922 mmol) was added in four equal increments every 3 min. After another 30 min of stirring at room temperature, TEOS (19.3 mg, 92.5 μ mol) and APTES (20.5 mg, 92.5 μ mol) were added to the reaction. The resulting mixture was then allowed to stir at room temperature overnight. After addition of ethanol (100 mL), the MSNs were collected by centrifugation (19 000 rpm, 43 146 rcf, for 20 min) and redispersed in absolute ethanol. The template extraction was performed by heating the MSN suspension under reflux (90 °C, oil bath temperature) for 45 min in an ethanolic solution (100 mL) containing NH₄NO₃ (2 g), followed

We show that MMP9-sensitive MSNs encapsulating cisplatin cause significant apoptosis in human lung tumor 3D-LTCs but not in healthy human lung tissue 3D-LTCs. This effect was MMP9 sequence specific, as no apoptosis was induced for MSNs containing noncleavable linkers encapsulating the same cisplatin concentration. To our knowledge, we are the first to show the effectiveness of MMP9-responsive drug delivery to human patient-derived tissue.

In summary, this study shows the feasibility of MMP9-mediated drug release in human lung tissue and in an advanced mouse model (*Kras* mutant mice) that closely reflects the human pathophysiology. Specifically, our novel drug delivery system using MMP9-responsive MSNs could be used to effectively deliver a combination of two drugs, bortezomib and cisplatin, in a stimuli-controlled manner and potentiate a synergistic effect selectively to (metastatic) tumors in mouse and human *ex vivo* tissue slices.

by 45 min heating under reflux in a mixture of concentrated HCl (10 mL) and absolute ethanol (90 mL). The mesoporous silica nanoparticles were collected by centrifugation and washed with absolute ethanol after each extraction step.

Heptapeptide Functionalization (MSN_{HP} and MSN_{NHP}). Biotin-PLGMWSR (HP-biotin 96.3%, 5.1 mg, 4.6 μ mol) or Biotin-PLLMWSR (NHP-biotin, 90.1%, 5.0 mg, 4.0 μ mol) were dissolved in 100 μ L of DMSO. The solution was diluted by addition of 400 μ L of H₂O. Then, EDC (0.8 mg, 5.2 μ mol) was added, and the reaction mixture was stirred for 5 min at room temperature. Subsequently, sulfoNHS (1 mg, 5.0 μ mol) was added, and the reaction mixture was stirred for another 5 min at room temperature. This mixture was added to a suspension containing 50 mg of sample MSN (NH₂ on the surface) in a total volume of 8 mL (EtOH/H₂O, 1:1). The resulting mixture was then allowed to stir at room temperature overnight. The MSNs were thoroughly washed with EtOH and H₂O (3 times) and finally collected by centrifugation (19 000 rpm, 43 146 rcf, 20 min). The HP-biotin- or NHP-biotin-functionalized MSNs were stored as a colloidal suspension in absolute ethanol.

Cargo Loading. One milligram of MSNs (MSN_{HP} or MSN_{NHP}) was immersed in 500 μ L of HBSS buffer containing fluorescein disodium salt dihydrate (1 mM), calcein-AM (20 or 50 μ M), cisplatin (2, 10, 20, or 100 μ M), or a combination of cisplatin and Bz (2 + 1 μ M, 10 + 1 μ M, or 20 + 1 μ M) for 2 h at room temperature. Afterwards, the particles were coated with avidin. Fluorescein-loaded particles were washed once by centrifugation and redispersion prior to the addition of avidin. All other samples were coated with avidin without a previous washing procedure.

Avidin Capping (cMSN and ncMSN). One milligram of loaded or nonloaded MSNs (in 500 μ L of HBSS buffer) was added to 500 μ L of HBSS buffer containing 1 mg of avidin. The solution was mixed by vortexing for 5 s and allowed to react for 30 min under static conditions at room temperature. The resulting suspension was then centrifuged (5000 rpm, 2200 rcf, 4 min, 15 °C) and washed three times with HBSS buffer. The particles were finally redispersed in HBSS buffer and used for *cuvette* release experiments or *in vitro* studies.

For details on characterization of the MSNs, please refer to the Supporting Information.

Cell Culture. The human non-small-cell lung cancer cell lines, A549 and H1299, were obtained from ATCC (American Type Culture Collection, Manassas, VA, USA). Both cell lines were maintained in DMEM media (Gibco, Life Technologies). Media were supplemented with 10% fetal bovine serum and 1%

penicillin/streptomycin. All cells were grown at 37 °C in a sterile humidified atmosphere containing 5% CO₂.

WST-1 Assay. The cytotoxicity of the nonloaded MSNs was assessed using the WST-1 assay (Roche). Briefly, 1.5×10^4 cells/well were seeded in 96-well plates. Twenty-four hours after seeding, the cells were exposed to cMSNs for 24 to 72 h. After treatment, 10 μ L of WST-1 reagent solution (Roche) was added to each well, and the cells were incubated at 37 °C for 30 min. Absorbance was measured at 450 nm using a Tristar LB 941 plate-reader (Berthold Technologies).

MTT Assay. The MTT assay was performed to assess cell viability after cisplatin or Bz release from the particles. Briefly, 1×10^4 cells/well for H1299 and 0.5×10^4 cells/well for A549 were seeded in 96-well plates. Forty-eight hours after seeding, cells were exposed to 50 μ g/mL MSN particles that had been loaded with solutions of cisplatin with or without Bz, in the presence of 0, 0.5, or 1 μ g/mL of recombinant MMP9 (Enzo Life Sciences) in 50 μ L of fresh media. In the case of transfected cells, 24 h after seeding, the cells were transfected with 0.15 μ g of MMP9 cDNA (DNASU) or empty vector cDNA per well using SatisFaction transfection reagent (Agilent Technologies), according to the manufacturer's instructions. Twenty-four hours after transfection, the cells were exposed to 50 μ g/mL cMSN particles that had been loaded with solutions of cisplatin, in 50 μ L of fresh media. After treatment, 10 μ L of a freshly prepared solution of 5 mg of thiazolyl blue tetrazolium bromide/mL of PBS (Sigma) was added to each well, and the cells were incubated at 37 °C for 1 h. The supernatant was then aspirated, and the violet crystals were dissolved in 500 μ L of 2-propanol + 0.1% Triton X-100. Absorbance was measured at 570 nm, using a Tristar LB 941 plate-reader (Berthold Technologies). Experiments were done in triplicate. Data analyses were performed in Prism Graphpad (version 6) software.

Zymography. To assess catalytically active MMP9 expression and transfection efficiency in A549 and H1299 cells, gelatin zymography was performed. In short, collected cell culture supernatants were centrifuged to get rid of cellular debris and then electrophoresed on 10% SDS-gels containing 1% gelatin substrate in nonreducing conditions (*i.e.*, no β -mercaptoethanol), so that the proteins could renature afterwards. After electrophoresis, the enzymes were renatured by incubation with 2.5% Triton-X-100 in developing buffer (50 mM Tris, 200 mM NaCl, 5 mM CaCl₂, pH 7.5) for 1 h at room temperature, to ensure that the proteins were catalytically active. Then, the gels were incubated in developing buffer at 37 °C for 24 h, to allow for the enzyme reaction to proceed. Thereafter, the gels were stained using PAGE-Blue (Fermentas) protein staining, according to the manufacturer's instructions. Gels were analyzed using the ChemiDoc XRS+ software (BioRad).

Animals. 129Sv-Kras^{tm3Tyj/J} (K-ras^{LA2}) mutant mice were obtained from The Jackson Laboratory, Bar Harbor, ME, USA, and cross-bred with FVB-NCrl WT females obtained from Charles River Laboratories, Sulzfeld, Germany, for seven generations. Animals were kept in rooms maintained at constant temperature and humidity with a 12/12 h light/dark cycle and were allowed food and water *ad libitum*. All procedures were conducted according to the international guidelines and with the approval of the Bavarian Animal Research Authority in Germany.

Human Tissue. The experiments with human tissue were approved by the Ethics Committee of the Ludwig-Maximilians-University Munich, Germany (LMU, project no. 455-12). All samples were provided by the Asklepios Biobank for Lung Diseases, Gauting, Germany (project no. 333-10). Written informed consent was obtained from all subjects. Tumor or tumor-free tissue from patients who underwent lung tumor resection was used.

Human and Mouse 3D Lung Tissue Cultures (3D-LTC). The whole procedure was done under sterile conditions and performed according to a method established by Uhl *et al.* (unpublished). WT FVB as well as Kras mutant mice with lung tumor burden were anaesthetized with a mixture of ketamine and xylazine hydrochloride (Bela-pharm, Germany). Kras mice of approximately 3 months of age that had several tumor lesions in each

lung tissue slice were used. After intubation and diaphragm dissection, lungs were perfused *via* the right ventricle with sodium chloride solution (Braun Vet Care, Germany). Using a syringe pump, airways were filled with warm 2 wt % low-melting agarose solution (Sigma, Germany) prepared in DMEM/F12 (Gibco, Germany) supplemented with 1% penicillin/streptomycin and amphotericin B (Sigma, Germany). Later, tracheae were knotted with a thread to keep the liquid agarose inside the airways. Afterward, the lungs were excised and transferred into tubes loaded with cultivation medium, left to cool on ice to allow for the solidification of the agarose. Finally, lobes were separated and cut with a vibratome (Hydrax V55, Zeiss, Germany) to a thickness of 200 μ m. The 3D-LTCs were cultivated for up to 3 days. The amount of sections per mouse varied between 30 and 50 slices. Directly after cutting, mouse 3D-LTCs were exposed to 50 μ g/mL of CP, CT, or Atto 633 labeled MSN particles containing CP or CT, administered directly into the medium. For human 3D-LTCs, tumorous and tumor-free regions excised from lung cancer surgeries were used. Airways at tumor-free segments were filled with 3 wt % agarose dissolved in DMEM/F12 as described above, *via* respective bronchi. Both the tumorous and tumor-free segments were then cut to a thickness of 300 μ m with the vibratome. Directly after cutting, mouse and human 3D-LTCs were exposed to 50 μ g/mL of MSN particles containing CP or CT, administered directly into the medium for 24–72 h.

Immunofluorescence. 3D-LTCs were fixed with acetone/methanol, 50/50 vol % solution for 10 min, washed with PBS, blocked for 1 h with Roti-ImmunoBlock (Carl Roth, Germany) at room temperature, and incubated with primary antibody at 4 °C overnight. Afterward, 3D-LTCs were washed with PBS, incubated with secondary antibody for 2 h at room temperature, again washed with PBS, and finally stained with DAPI. Stained 3D-LTCs were mounted using fluorescence mounting medium (DAKO, USA) and evaluated using confocal microscopy (LSM710, Carl Zeiss, Germany). 3D reconstruction and quantification of cell death in the 3D-LTC were conducted using the IMARISx64 software (version 7.6.4, Bitplane, Switzerland). Maximum intensity projections were made using ZEN2009 software (Carl Zeiss, Germany).

Immunohistochemistry. Lung segments were placed in 4% (w/v) paraformaldehyde after excision and processed for paraffin embedding. 3 μ m thick sections on slides were subjected to quenching of endogenous peroxidase activity using a mixture of methanol/H₂O₂ for 20 min, followed by antigen retrieval in a decloaking chamber. From this step on, the slides were washed with TBST after each incubation with the reagents throughout the procedure. The sections were incubated first with Rodent Block M (Zytomed Systems, Germany) for 30 min and then with the primary antibody, *i.e.*, MMP9 (Millipore, USA) or IgG, control for 1 h. The cuts were then incubated with Rabbit on Rodent AP-Polymer for 30 min, which was followed by Vulcan Fast Red, AP substrate solution (both Biocare Medical, Concord, USA) incubation for 10–15 min. The sections were counterstained with hematoxylin (Carl Roth, Germany) and dehydrated respectively in consecutively grading ethanol and xylene (both Appli-Chem, Germany) incubations. Dried slides were mounted in Entellan (Merck, Germany).

Study Design and Statistics. The therapeutic effect of the particles was assessed by immunofluorescent stainings using an apoptosis marker (cleaved caspase-3) and was investigated on lung tissue slices from 15 different Kras mutant animals that were prepared and exposed to the MSNs or free drugs in three independent experiments. Similarly sized tumors were chosen for the imaging from a minimum of three different mice per individual staining. In addition, each staining was performed a minimum of three times per mouse. Three representative images of three different mice were chosen for the quantification as shown in Figure 4. The quantification was done blinded using the IMARISx64 software (version 7.6.4, Bitplane, Switzerland). For the controls, nine WT FVB mice lungs were prepared in three independent experiments and stained and quantified according to the same principle. For comparison of two groups, one-way ANOVA analysis was performed. A *p*-value lower than 0.05 was considered statistically significant

Western Blotting. Human 3D-LTCs were lysed in RIPA buffer (50 mM Tris HCl, pH 7.5, 150 mM NaCl, 1% NP40, 0.5% sodium deoxycholate, 0.1% SDS) supplemented with protease inhibitor cocktail (Complete, Roche). Protein content was determined using the Pierce BCA protein assay kit (Thermo Scientific). For Western blot analysis, equal amounts of protein were subjected to electrophoresis on 12% SDS-PAGE gels and blotted onto PVDF membranes. Membranes were treated with antibodies using standard Western blot techniques. The ECL Plus detection reagent (GE Healthcare) was used for chemiluminescent detection, and membranes were analyzed with the ChemiDoc XRS+ (Bio-Rad).

Conflict of Interest: The authors declare no competing financial interest.

Supporting Information Available: Materials and methods, additional characterization techniques (Figure S1), cell survival curve with cisplatin in A549 and H1299 cells, gelatin zymogram (Figure S2). Stimulated release of calcein-AM from MSNs (Figure S3). Experimental setup of 3D-LTC (Figure S4). WT 3D-LTC exposed to cMSN and nonencapsulated drugs (Figure S5). Confocal microscopy images for $n = 3$ *Kras* mutant mouse 3D-LTC exposed to free drugs and MSNs for 24 h (Figure S6) and 48 h (Figure S7). *Kras* 3D-LTC exposed to Bz alone, MMP9, and E-cadherin containing in *Kras* 3D-LTC exposed to MSNs, calculated amount of particles, nuclei, and apoptotic cells in 3D-LTC after different treatments (Figure S8). This material is available free of charge via the Internet at <http://pubs.acs.org>.

Acknowledgment. We thank the Alexander von Humboldt Foundation for providing funding for S.H.v.R. Furthermore, financial support from the Nanosystems Initiative Munich (NIM), the Center for NanoScience Munich (CeNS), and the DFG (SFB 749) are gratefully acknowledged. In addition, this study was supported by an ERC Starting Grant to M.K. (ERC-StG Grant No. 261302). We thank Dr. B. Rühle for the 3D graphics design, F. Uhl for help with tissue slicing, Dr. G. Burgstaller for help with imaging, N. Semren for help with the *Kras* mutant mouse model, and I. Keller for help with immunohistochemistry.

REFERENCES AND NOTES

- Malam, Y.; Lim, E. J.; Seifalian, A. M. Current Trends in the Application of Nanoparticles in Drug Delivery. *Curr. Med. Chem.* **2011**, *18*, 1067–1078.
- Egeblad, M.; Werb, Z. New Functions for the Matrix Metalloproteinases in Cancer Progression. *Nat. Rev. Cancer* **2002**, *2*, 161–174.
- Gialeli, C.; Theocharis, A. D.; Karamanos, N. K. Roles of Matrix Metalloproteinases in Cancer Progression and Their Pharmacological Targeting. *FEBS J.* **2011**, *278*, 16–27.
- Iniesta, P.; Moran, A.; De Juan, C.; Gomez, A.; Hernando, F.; Garcia-Aranda, C.; Frias, C.; Diaz-Lopez, A.; Rodriguez-Jimenez, F. J.; Balibrea, J. L.; *et al.* Biological and Clinical Significance of Mmp-2, Mmp-9, Timp-1 and Timp-2 in Non-Small Cell Lung Cancer. *Oncol. Rep.* **2007**, *17*, 217–223.
- Martins, S. J.; Takagaki, T. Y.; Silva, A. G.; Gallo, C. P.; Silva, F. B.; Capelozzi, V. L. Prognostic Relevance of Ttf-1 and Mmp-9 Expression in Advanced Lung Adenocarcinoma. *Lung Cancer* **2009**, *64*, 105–109.
- Turk, B. E.; Huang, L. L.; Piro, E. T.; Cantley, L. C. Determination of Protease Cleavage Site Motifs Using Mixture-Based Oriented Peptide Libraries. *Nat. Biotechnol.* **2001**, *19*, 661–667.
- Li, H.; Yu, S. S.; Miteva, M.; Nelson, C. E.; Werfel, T.; Giorgio, T. D.; Duvall, C. L. Matrix Metalloproteinase Responsive, Proximity-Activated Polymeric Nanoparticles for siRNA Delivery. *Adv. Funct. Mater.* **2013**, *23*, 3040–3052.
- Chien, M. P.; Carlini, A. S.; Hu, D. H.; Barback, C. V.; Rush, A. M.; Hall, D. J.; Orr, G.; Gianneschi, N. C. Enzyme-Directed Assembly of Nanoparticles in Tumors Monitored by in Vivo Whole Animal Imaging and ex Vivo Super-Resolution Fluorescence Imaging. *J. Am. Chem. Soc.* **2013**, *135*, 18710–18713.
- Yamada, R.; Kostova, M. B.; Anchoori, R. K.; Xu, S.; Neamati, N.; Khan, S. R. Biological Evaluation of Paclitaxel-Peptide Conjugates as a Model for Mmp2-Targeted Drug Delivery. *Cancer Biol. Ther.* **2010**, *9*, 192–203.
- Zhu, L.; Kate, P.; Torchilin, V. P. Matrix Metalloprotease 2-Responsive Multifunctional Liposomal Nanocarrier for Enhanced Tumor Targeting. *ACS Nano* **2012**, *6*, 3491–3498.
- Chien, M. P.; Thompson, M. P.; Barback, C. V.; Ku, T. H.; Hall, D. J.; Gianneschi, N. C. Enzyme-Directed Assembly of a Nanoparticle Probe in Tumor Tissue. *Adv. Mater.* **2013**, *25*, 3599–3604.
- Gu, G.; Xia, H.; Hu, Q.; Liu, Z.; Jiang, M.; Kang, T.; Miao, D.; Tu, Y.; Pang, Z.; Song, Q.; *et al.* Peg-Co-Pcl Nanoparticles Modified with Mmp-2/9 Activatable Low Molecular Weight Protamine for Enhanced Targeted Glioblastoma Therapy. *Biomaterials* **2013**, *34*, 196–208.
- Hatakeyama, H.; Akita, H.; Ito, E.; Hayashi, Y.; Oishi, M.; Nagasaki, Y.; Danev, R.; Nagayama, K.; Kaji, N.; Kikuchi, H.; *et al.* Systemic Delivery of siRNA to Tumors Using a Lipid Nanoparticle Containing a Tumor-Specific Cleavable PEG-Lipid. *Biomaterials* **2011**, *32*, 4306–4316.
- Argyó, C.; Weiss, V.; Bräuchle, C.; Bein, T. Multifunctional Mesoporous Silica Nanoparticles as a Universal Platform for Drug Delivery. *Chem. Mater.* **2014**, *26*, 435–451.
- Li, Z.; Barnes, J. C.; Bosoy, A.; Stoddart, J. F.; Zink, J. I. Mesoporous Silica Nanoparticles in Biomedical Applications. *Chem. Soc. Rev.* **2012**, *41*, 2590–2605.
- Cauda, V.; Schlossbauer, A.; Kecht, J.; Zurner, A.; Bein, T. Multiple Core-Shell Functionalized Colloidal Mesoporous Silica Nanoparticles. *J. Am. Chem. Soc.* **2009**, *131*, 11361–11370.
- Sauer, A. M.; Schlossbauer, A.; Ruthardt, N.; Cauda, V.; Bein, T.; Bräuchle, C. Role of Endosomal Escape for Disulfide-Based Drug Delivery from Colloidal Mesoporous Silica Evaluated by Live-Cell Imaging. *Nano Lett.* **2010**, *10*, 3684–3691.
- Zhao, Y. L.; Li, Z.; Kabehie, S.; Botros, Y. Y.; Stoddart, J. F.; Zink, J. I. pH-Operated Nanopistons on the Surfaces of Mesoporous Silica Nanoparticles. *J. Am. Chem. Soc.* **2010**, *132*, 13016–13025.
- Giri, S.; Trewyn, B. G.; Stellmaker, M. P.; Lin, V. S. Y. Stimuli-Responsive Controlled-Release Delivery System Based on Mesoporous Silica Nanorods Capped with Magnetic Nanoparticles. *Angew. Chem., Int. Ed.* **2005**, *44*, 5038–5044.
- Aznar, E.; Mondragon, L.; Ros-Lis, J. V.; Sancenón, F.; Marcos, M. D.; Martínez-Manez, R.; Soto, J.; Pérez-Paya, E.; Amoros, P. Finely Tuned Temperature-Controlled Cargo Release Using Paraffin-Capped Mesoporous Silica Nanoparticles. *Angew. Chem., Int. Ed.* **2011**, *50*, 11172–11175.
- Popat, A.; Liu, J.; Lu, G. Q.; Qiao, S. Z. A pH-Responsive Drug Delivery System Based on Chitosan Coated Mesoporous Silica Nanoparticles. *J. Mater. Chem.* **2012**, *22*, 11173–11178.
- Schlossbauer, A.; Kecht, J.; Bein, T. Biotin-Avidin as a Protease-Responsive Cap System for Controlled Guest Release from Colloidal Mesoporous Silica. *Angew. Chem., Int. Ed.* **2009**, *48*, 3092–3095.
- Mackowiak, S. A.; Schmidt, A.; Weiss, V.; Argyó, C.; von Schirnding, C.; Bein, T.; Bräuchle, C. Targeted Drug Delivery in Cancer Cells with Red-Light Photoactivated Mesoporous Silica Nanoparticles. *Nano Lett.* **2013**, *13*, 2576–2583.
- Bae, M.; Cho, S.; Song, J.; Lee, G. Y.; Kim, K.; Yang, J.; Cho, K.; Kim, S. Y.; Byun, Y. Metalloprotease-Specific Poly(Ethylene Glycol) Methyl Ether-Peptide-Doxorubicin Conjugate for Targeting Anticancer Drug Delivery Based on Angiogenesis. *Drugs Exp. Clin. Res.* **2003**, *29*, 15–23.
- Bauvois, B. New Facets of Matrix Metalloproteinases MMP-2 and MMP-9 as Cell Surface Transducers: Outside-in Signaling and Relationship to Tumor Progression. *Biochim. Biophys. Acta* **2012**, *1825*, 29–36.
- Cauda, V.; Schlossbauer, A.; Bein, T. Bio-Degradation Study of Colloidal Mesoporous Silica Nanoparticles: Effect of Surface Functionalization with Organo-Silanes and Poly(Ethylene Glycol). *Microporous Mesoporous Mater.* **2010**, *132*, 60–71.
- Cauda, V.; Argyó, C.; Bein, T. Impact of Different Pegylation Patterns on the Long-Term Bio-Stability of Colloidal

- Mesoporous Silica Nanoparticles. *J. Mater. Chem.* **2010**, *20*, 8693–8699.
28. Dubey, S.; Powell, C. A. Update in Lung Cancer 2007. *Am. J. Respir. Crit. Care Med.* **2008**, *177*, 941–946.
 29. Davies, A. M.; Lara, P. N., Jr.; Mack, P. C.; Gandara, D. R. Incorporating Bortezomib into the Treatment of Lung Cancer. *Clin. Cancer Res.* **2007**, *13*, s4647–4651.
 30. Besse, B.; Planchard, D.; Veillard, A. S.; Taillade, L.; Khayat, D.; Ducourtieux, M.; Pignon, J. P.; Lombroso, J.; Lafontaine, C.; Mathiot, C.; *et al.* Phase 2 Study of Frontline Bortezomib in Patients with Advanced Non-Small Cell Lung Cancer. *Lung Cancer* **2012**, *76*, 78–83.
 31. Johnson, L.; Mercer, K.; Greenbaum, D.; Bronson, R. T.; Crowley, D.; Tuveson, D. A.; Jacks, T. Somatic Activation of the K-Ras Oncogene Causes Early Onset Lung Cancer in Mice. *Nature* **2001**, *410*, 1111–1116.
 32. Mills, N. E.; Fishman, C. L.; Rom, W. N.; Dubin, N.; Jacobson, D. R. Increased Prevalence of K-Ras Oncogene Mutations in Lung Adenocarcinoma. *Cancer Res.* **1995**, *55*, 1444–1447.
 33. Cancer Genome Atlas Network. Comprehensive Molecular Profiling of Lung Adenocarcinoma. *Nature* **2014**, *511*, 543–550.
 34. The Clinical Lung Cancer Genome Project (CLCGP) and Network Genomic Medicine (NGM). A Genomics-Based Classification of Human Lung Tumors. *Sci. Trans. Med.* **2013**, *5*, 209ra153.
 35. Dasari, S.; Bernard Tchounwou, P. Cisplatin in Cancer Therapy: Molecular Mechanisms of Action. *Eur. J. Pharmacol.* **2014**, *740C*, 364–378.
 36. Rink, J. S.; Plebanek, M. P.; Tripathy, S.; Thaxton, C. S. Update on Current and Potential Nanoparticle Cancer Therapies. *Curr. Opin. Oncol.* **2013**, *25*, 646–651.
 37. Taratula, O.; Garbuzenko, O. B.; Chen, A. M.; Minko, T. Innovative Strategy for Treatment of Lung Cancer: Targeted Nanotechnology-Based Inhalation Co-delivery of Anticancer Drugs and siRNA. *J. Drug Targeting* **2011**, *19*, 900–914.
 38. Kulkarni, P. S.; Haldar, M. K.; Nahire, R. R.; Katti, P.; Ambre, A. H.; Muhonen, W. W.; Shabb, J. B.; Padi, S. K.; Singh, R. K.; Borowicz, P. P.; *et al.* MMP-9 Responsive PEG Cleavable Nanovesicles for Efficient Delivery of Chemotherapeutics to Pancreatic Cancer. *Mol. Pharmaceutics* **2014**, *11*, 2390–2399.
 39. Liu, Q.; Li, R. T.; Qian, H. Q.; Yang, M.; Zhu, Z. S.; Wu, W.; Qian, X. P.; Yu, L. X.; Jiang, X. Q.; Liu, B. R. Gelatinase-Stimuli Strategy Enhances the Tumor Delivery and Therapeutic Efficacy of Docetaxel-Loaded Poly(Ethylene Glycol)-Poly-(Varepsilon-Caprolactone) Nanoparticles. *Int. J. Nanomed.* **2012**, *7*, 281–295.
 40. Singh, N.; Karambelkar, A.; Gu, L.; Lin, K.; Miller, J. S.; Chen, C. S.; Sailor, M. J.; Bhatia, S. N. Bioresponsive Mesoporous Silica Nanoparticles for Triggered Drug Release. *J. Am. Chem. Soc.* **2011**, *133*, 19582–19585.
 41. Zhang, J.; Yuan, Z. F.; Wang, Y.; Chen, W. H.; Luo, G. F.; Cheng, S. X.; Zhuo, R. X.; Zhang, X. Z. Multifunctional Envelope-Type Mesoporous Silica Nanoparticles for Tumor-Triggered Targeting Drug Delivery. *J. Am. Chem. Soc.* **2013**, *135*, 5068–5073.
 42. Xu, J. H.; Gao, F. P.; Li, L. L.; Ma, H. L.; Fan, Y. S.; Liu, W.; Guo, S. S.; Zhao, X. Z.; Wang, H. Gelatin-Mesoporous Silica Nanoparticles as Matrix Metalloproteinases-Degradable Drug Delivery Systems in Vivo. *Microporous Mesoporous Mater.* **2013**, *182*, 165–172.
 43. Neuhaus, V.; Schwarz, K.; Klee, A.; Seehase, S.; Forster, C.; Pfennig, O.; Jonigk, D.; Fieguth, H. G.; Koch, W.; Warnecke, G.; *et al.* Functional Testing of an Inhalable Nanoparticle Based Influenza Vaccine Using a Human Precision Cut Lung Slice Technique. *PLoS One* **2013**, *8*, e71728.
 44. Paranjpe, M.; Neuhaus, V.; Finke, J. H.; Richter, C.; Gothsch, T.; Kwade, A.; Buttgenbach, S.; Braun, A.; Muller-Goymann, C. C. In Vitro and Ex Vivo Toxicological Testing of Sildenafil-Loaded Solid Lipid Nanoparticles. *Inhalation Toxicol.* **2013**, *25*, 536–543.
 45. Nassimi, M.; Schleh, C.; Lauenstein, H. D.; Hussein, R.; Lubbers, K.; Pohlmann, G.; Switalla, S.; Sewald, K.; Muller, M.; Krug, N.; *et al.* Low Cytotoxicity of Solid Lipid Nanoparticles in In Vitro and Ex Vivo Lung Models. *Inhalation Toxicol.* **2009**, *21* (Suppl 1), 104–109.
 46. Uberall, I.; Kolar, Z.; Trojanec, R.; Berkovcova, J.; Hajduch, M. The Status and Role of ErbB Receptors in Human Cancer. *Exp. Mol. Pathol.* **2008**, *84*, 79–89.
 47. Eberhard, D. A.; Johnson, B. E.; Amler, L. C.; Goddard, A. D.; Heldens, S. L.; Herbst, R. S.; Ince, W. L.; Janne, P. A.; Januario, T.; Johnson, D. H.; *et al.* Mutations in the Epidermal Growth Factor Receptor and in Kras Are Predictive and Prognostic Indicators in Patients with Non-Small-Cell Lung Cancer Treated with Chemotherapy Alone and in Combination with Erlotinib. *J. Clin. Oncol.* **2005**, *23*, 5900–5909.
 48. Cappuzzo, F.; Varella-Garcia, M.; Finocchiaro, G.; Skokan, M.; Gajapathy, S.; Carnaghi, C.; Rimassa, L.; Rossi, E.; Ligorio, C.; Di Tommaso, L.; *et al.* Primary Resistance to Cetuximab Therapy in Egfr Fish-Positive Colorectal Cancer Patients. *Br. J. Cancer* **2008**, *99*, 83–89.
 49. Roy, R.; Yang, J.; Moses, M. A. Matrix Metalloproteinases as Novel Biomarkers and Potential Therapeutic Targets in Human Cancer. *J. Clin. Oncol.* **2009**, *27*, 5287–5297.
 50. Itoh, T.; Tanioka, M.; Matsuda, H.; Nishimoto, H.; Yoshioka, T.; Suzuki, R.; Uehira, M. Experimental Metastasis Is Suppressed in MMP-9-Deficient Mice. *Clin. Exp. Metastasis* **1999**, *17*, 177–181.
 51. Davies, A. M.; Lara, P. N.; Lau, D. H.; Mack, P. C.; Gumerlock, P. H.; Gandara, D. R.; Schenkein, D.; Doroshow, J. H. The Proteasome Inhibitor, Bortezomib, in Combination with Gemcitabine (Gem) and Carboplatin (Carbo) in Advanced Non-Small Cell Lung Cancer (Nslcl): Final Results of a Phase I California Cancer Consortium Study. *J. Clin. Oncol.* **2004**, *22*, 642s–642s.